



# Liquid blockage and flow maldistribution of two-phase flow in two parallel thin micro-channels

Jingtian Wu, Yun Wang<sup>\*</sup>

Renewable Energy Resources Lab (RERL), Department of Mechanical and Aerospace Engineering, University of California, Irvine, CA 92697-3975, United States

## ARTICLE INFO

### Keywords:

Micro-channel  
Thin channel  
Two-phase flow  
Maldistribution  
Experiment  
Instability

## ABSTRACT

In this study, flow maldistribution in a system of two parallel thin micro-channels with shared inlet and outlet manifolds is experimentally investigated with one channel subject to single-phase flow and the other to two-phase one. The flow pattern, pressure drop, gas flow rate in the single-phase flow channel  $Q_1$  and two-phase flow channel  $Q_2$  are studied. Film flow patterns are observed for all the cases of the study, consistent with literature work. The  $\frac{Q_2}{Q_1}$  ratio is defined as a direct measure to flow maldistribution. Theoretical derivation shows that  $\frac{Q_2}{Q_1}$  is inverse of the two-phase multiplier  $\phi$  or  $\frac{Q_2}{Q_1} = \frac{1}{\phi}$ . Three levels of liquid flow rate are examined and presented to show three representative trends: (1) For the highest water flow rate, i.e.  $10^{-2}$  m/s,  $\frac{Q_2}{Q_1}$  is found to monotonically increase with the air flow rate, with its value  $\frac{Q_2}{Q_1}$  as low as about 0.2 at 0.86 m/s gas velocity and approaching 0.65 at 3.44 m/s. (2) For the lowest water velocity, i.e.  $10^{-4}$  m/s,  $\frac{Q_2}{Q_1}$  shows decrease at first, followed by an increase, as the superficial gas velocity increases from 0.86 m/s to 3.44 m/s. It reaches about 0.76 at 0.86 m/s gas velocity and drops to about 0.55 at 1.72 m/s. (3) For the intermediate water velocity, i.e.  $10^{-3}$  m/s, two “steady” states are identified at 0.86 m/s gas velocity with one having  $\frac{Q_2}{Q_1}$  as high as about 0.69 and the other about 0.52. The rest follows a similar trend as  $10^{-4}$  m/s liquid velocity. The observed two “steady” states and changing trend at the two low liquid velocities may be due to the altered liquid blockage near the channel exit. It is also indicated that the two-phase multiplier  $\phi$  obtained in single channel testing may not be used to measure flow maldistribution in multiple-channel systems. The work is important to study of two-phase flow, multi-channel design, flow maldistribution, and flow control in micro-channels for PEM fuel cells, electrolyzers, and thermal devices.

## 1. Introduction

Micro-channels play a crucial role in many applications of engineering, such as PEM fuel cell gas channels [1–5], heat exchangers [6–8] and microfluidics [9,10]. In micro-channel heat exchangers for cooling, two-phase flow is capable of delivering a large amount of heat via phase change. The channels supply liquid to the hot channel surface, where boiling occurs to absorb heat, and remove vapor out of the channel [6,8]. In PEM fuel cells, gas flow channels with a cross-section of 0.3–1 mm are arranged usually in parallel-serpentine configurations to supply hydrogen fuel and oxygen reactants for electrochemical reactions. In addition, they are also used to remove byproduct water out of fuel cells to avoid electrode “flooding”. Fig. 1 shows the liquid water observed in the gas flow channels using optical method and neutron radiography.

Liquid water, originated from the water production of PEM fuel cell reactions, may block the channel reactant flow in a or several local channels, leading to flow maldistribution and reactant starvation in porous electrodes, which is a major source for fuel cell voltage loss and material degradation [11–15].

Two-phase flow dynamics in micro-channels have been widely studied in both heat exchanger and PEM fuel cell. Cubaud et al. [18] investigated the shape of static elongated bubbles in square channels for different contact angles. They found that dynamic contact angles play an important role in the selection of flow regime. Zhao et al. [19] experimentally investigated the flow of immiscible fluids (water and kerosene) in a microchannel 300  $\mu\text{m}$  wide and 600  $\mu\text{m}$  deep. The experimental data of volume of dispersed phase were correlated as a function of  $W_{e,KS}$ . Cho and Wang experimentally and numerically studied two-phase flows in a

<sup>\*</sup> Corresponding author.

E-mail address: [yunw@uci.edu](mailto:yunw@uci.edu) (Y. Wang).

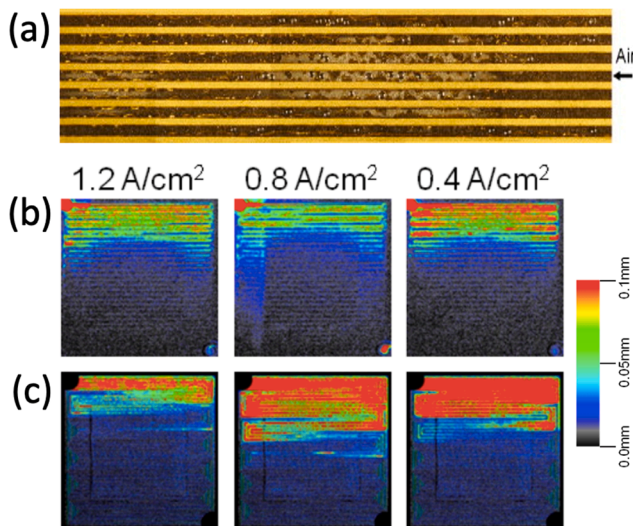


**Fig. 1.** (a) Two-phase flow in parallel gas flow channels of operating PEM fuel cells using in-situ direct optical method [16], (b) liquid water in single serpentine flow channels, and (c) in 4-parallel channel arranged in serpentine of PEM fuel cells using in-situ neutron radiography [17]. The color scale on the right shows the liquid water thickness.

micro-channel with hydrophilic [20] and heterogeneous [21] surfaces, and found that both surface wettability and roughness affect the location of the liquid water flow, flow patterns, and pressure drop. Lee et al. [22] experimentally investigated bubble dynamics in a single trapezoid microchannel with the hydraulic diameter of  $41.3 \mu\text{m}$ . They concluded that the size of bubble detaching the channel wall is governed by the surface tension and drag of bulk flow, and bubble frequency in the microchannel is comparable to that in an ordinary size channel. Bowers and Mudawar [23] explored the increased rate of heat dissipation from electronic chips using flow boiling in mini-/micro-channels. They found that the flow acceleration resulting from evaporation is a major contributor to the pressure drop in the channels, and compressibility effects are significant in the micro-channels. Peles [24] conducted experiment to investigate the mechanisms associated with microscale forced convection in boiling two-phase flow. Various flow regimes were observed, including rapid bubble growth, complete bubble flow, bubbly flow and annular flow. They found that increasing the system and pump frequencies decreases the temperature fluctuation. Cheng and Wu [25] reviewed phase-change heat transfer in microsystems, including flow boiling and condensation in microchannels as well as bubble growth and collapse. For boiling in microchannels, it was found that single- and two-phase alternating flows with large fluctuation of pressure and temperature exist at low mass fluxes with a high degree of inlet subcooling. Ravigururajan [26] conducted subcooled and saturated flow boiling experiment using a diamond-pattern microchannel heat exchanger. They inferred that heat transfer coefficients are influenced by the flow rates, wall superheat and value of quality, and the pressure drop decreases rapidly for an increasing heat transfer coefficient. Salim et al. [27] investigated oil–water two-phase flows in microchannels of about  $700 \mu\text{m}$  hydraulic diameters. Different flow patterns were identified and mapped with pressure drops measured. They found that the pressure drop strongly depends on flow rates, microchannel material and first fluid injected into the microchannel. Fu et al. [28] presented experimental investigation on Newtonian/non-Newtonian fluids two-phase flow in T-shaped rectangular microchannels. Four flow patterns were observed for cyclohexan/carboxyl methyl cellulose (CMC) solutions, including slug flow, droplet flow, parallel flow and jet flow. In general, mist flow, droplet formation, annulus, and slug flow are frequently observed in microchannels [29–31]. Adroher and Wang [32] investigated the patterns and pressure drop of air–water flows in the range of

PEM fuel cell operation, and developed a flow-pattern map of wavy, annulus, wavy-annulus and slug-annular regimes. They also observed unstable two-phase flow near the outlet.

Flow dynamics and maldistribution in parallel mini/micro-channels are a major topic in studying two-phase flow. In PEM fuel cells, flow maldistribution impairs cell performance dramatically by non-uniform distribution of reactants in multiple gas channels and liquid water accumulation in local channels, as shown in Fig. 1 [1]. Several attempts have been made to model and predict flow distribution in parallel channels of fuel cells [33–35]. Zhang found that flow maldistribution and hysteresis occur at low gas and liquid flow velocities in a parallel square mini-channel systems and the gravitational force greatly impacts flow distribution and hysteresis [36]. Zhang [37] studied flow patterns and pressure drop characteristics of two-phase flow in a Y-branched parallel channel system under fuel cell conditions. They concluded that even distribution of gas and liquid flow could always be achieved under sufficiently high gas/liquid velocities. Kandlikar [38] proposed a new technique to measure instantaneous flow rate in a parallel channel array. Using this method, the mass flow rate in each channel could be estimated from the pressure drop in the entrance region when the contraction loss coefficient  $K_c$  is known. Suman et al. [16] performed multiphase flow computations to examine the effects of gas diffusion layer (GDL) intrusion and manifold design on reducing flow maldistribution. They showed that two splitter plates in the header manifold can bring down the flow maldistribution. Flow maldistribution has a great impact on the performance of microchannel heat exchangers. Nielsen et al. [39] investigated the effect of flow maldistribution on the performance of microchannel heat exchanger both experimentally and numerically. They found that as the variation in individual channel thickness increases the heat exchanger performance decreases significantly. Anbumeenakshi and Thansekar [40] carried out experimental investigation to analyze flow maldistribution in a microchannel heat sink. They found that flow is more uniform with trapezoidal and triangular headers at low flow rates and with a rectangular header at higher rates. Seungwhan et al. [41] developed a heat exchanger model to study axial conduction and flow maldistribution's impact. They concluded that geometry modification of cross section and cross link in parallel channel is a solution to mitigate flow maldistribution. Wen et al. [42] studied flow characteristics in the entrance of a plate-fin heat exchanger using particle image velocimetry (PIV). They concluded that fluid maldistribution in the conventional entrance configuration is severe while the improved entrance configuration with punched baffle can effectively improve the performance of fluid flow in the entrance. Kumaraguruparan et al. [43] numerically and experimentally studied flow maldistribution in U-type micro-channel configuration, and indicated that decrease of the cross-sectional dimension and increase of the channel length reduce flow maldistribution.

Though several attempts have been made to study two-phase flow and flow maldistribution in multiple channels, the phenomena are complex and challenging partly due to unstable flow dynamics and impacts of heterogeneity, and needs further investigation, including additional experimental data, new testing methods, and rigorous theoretical analysis. As our first step to experimentally investigate the phenomena, we focus on two parallel channels, with one channel subject to single-phase gas flow and the other to two-phase one. The two parallel channels share the same inlet and outlet manifolds. This study leverages the specially designed experimental apparatus to visualize flow patterns, measure the pressure drop and gas flow rates in the two channels, respectively. We also define a parameter to directly measure flow maldistribution between the two channels, and derive a formula which directly relates this parameter to the two-phase multiplier. Two methods are proposed to experimentally obtain this parameter.

## 2. Experimental

To experimentally investigate the fundamentals of flow maldistribution

bution in a two-channel flow system, we consider a simplified experimental setup, as shown in Fig. 2, which depicts the design of the two-parallel thin micro-channels system. It consists of two identical micro-channels arranged in parallel and placed horizontally with a shared inlet manifold and their outlets connected to the ambient. Both channels have a rectangular cross-section of 0.324 mm by 3.00 mm with a total length of 178 mm. This channel dimension is similar to that of Refs. [46] and [48], which study two-phase flow in a single channel. The channel plate is made of 304 stainless steel, placed on a 6061 aluminum base. A polycarbonate window plate is placed on top for flow visualization. All the components were fabricated using a high-precision CNC milling machine. The micro-channel system is sealed by compression of bolts.

Fig. 3 schematically shows the experiment setup, including the two-channel system, inlet gas flow controller, liquid injection controller, pressure measurement unit, gas flow rate measurement units, and visualization camera. Two-phase flow is established by injecting liquid water into Channel 2, while Channel 1 remains in the single-phase flow regime without any water addition. The water injection port was located in the base plate with a diameter of 0.28 mm at a distance of 60 mm downstream from the air inlet. Thus, Channel 2 consists of a single-phase flow length before the port and a two-phase flow region after. A syringe pump (New Era Pump System NE-300) injects room temperature deionized water into Channel 2 at three flow rates, 0.3499, 3.499, and 34.99 ml/hour, corresponding to a superficial velocity of  $10^{-4}$ ,  $10^{-3}$  and  $10^{-2}$  m/s, respectively. A mass flow controller (SmartTrak 100) regulates seven air flow rates at room temperature ( $20 \text{ }^\circ\text{C} \pm 2 \text{ }^\circ\text{C}$ ) in the range of 100–400 ml/min ( $\pm 5$  ml/min), corresponding to a superficial velocity of 0.86–3.44 m/s. The inlets and outlets of the two channels share the same manifolds, ensuring the same pressure drop between the two micro-channels in all the testing conditions.

A pressure transducer (OMEGA PX 409) was employed to measure the pressure drop between the channel inlet and outlet. The flow patterns in the two-phase channel were captured by a DSLR camera (Canon Rebel T3). It takes about 10 min to 2 h depending on the air and water flow rates for the pressure drop to reach a steady state, when the measurements of flow rates were taken. Table 1 lists the operational conditions, physical properties of fluids and channel parameters.

### 3. Results and discussion

#### 3.1. Pressure and flow rates of single-phase flow in both micro-channels

To verify the cross-sectional areas and the identical dimension of Channel 1 and 2 in the experimental setup, single-phase flow testing was first conducted. In a channel, the single-phase pressure drop is theoretically given by [44]:

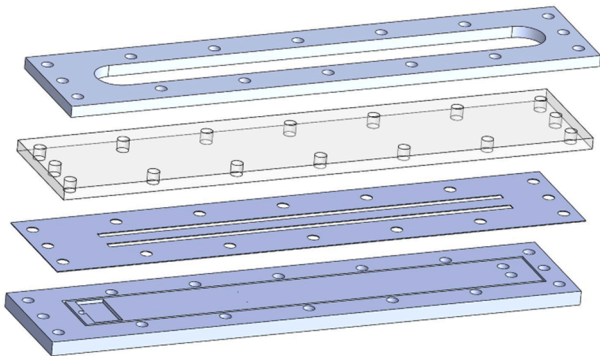


Fig. 2. Design and assembly of the two parallel micro-channels system (From top to bottom: O-shaped endplate, transparent plate, channel plate, and base plate).

$$\Delta P = \frac{fL\rho_g u_g^2}{2D_h} = \frac{fL\rho_g Q^2}{2D_h A^2} \quad \text{where } D_h = \frac{A}{L_p} \quad (1)$$

where  $f$ ,  $L$ ,  $\rho_g$ ,  $u_g$ ,  $A$ ,  $Q$ ,  $D_h$ , and  $L_p$  represent the friction factor, channel length, gas density, superficial gas velocity, cross-sectional area, flow rate, hydraulic diameter, and perimeter, respectively. In general, the friction factor is a function of the Reynold number in the laminar flow regime:

$$f = \frac{C}{Re} \quad (2)$$

For a rectangular channel,  $C$  is given by [45]:

$$C = 96\left(1 - 1.35532\left(\frac{1}{\alpha}\right) + 1.9467\left(\frac{1}{\alpha}\right)^2 - 1.7012\left(\frac{1}{\alpha}\right)^3 + 0.9564\left(\frac{1}{\alpha}\right)^4 - 0.2537\left(\frac{1}{\alpha}\right)^5\right) \quad (3)$$

where  $\alpha$  is the aspect ratio of the channel, defined as the ratio of the width ( $a$ ) to height ( $b$ ) in the cross-section.

In addition, Wang [51] proposed to treat micro-channels as a type of porous media with regular pore networks, thus Darcy's law applies:

$$u_g = -\frac{K}{\mu} \nabla P \quad (4)$$

where  $K$  is the permeability. This property of a porous medium measures the material ability to allow fluids to pass through it, which is related to the porosity and pore size as well as the shapes of the pores and their connectedness. For a constant cross-sectional area channel of a length  $L$ , one will reach:

$$\Delta P = \frac{\mu L}{K} u_g \quad (5)$$

By combining Eqs. (1) and (5), one will reach:

$$K = \frac{2\rho(D_h)^2}{C} \quad (6)$$

The pressure drops across Channel 1 and Channel 2, respectively, are always the same at steady state due to sharing of the inlet and the outlet manifolds. The superficial velocity is defined using the total flow rate and the cross-sectional area of the two channels. Fig. 4 compares the experimental data of the pressure drop with that of a single channel predicted by Eqs. (1) or (5). The deviation from the theoretical value is within 2% except for the highest velocity in which it is about 4%. The uncertainties in the pressure and gas flow measurements are 2 Pa and 0.043 m/s, respectively.

To verify the identical dimension of Channel 1 and Channel 2, the volumetric flow rates were measured in each of the two channels. For each condition, measurement of the air flow rates was repeated five times. Fig. 5 compares the air flow rates in the two channels under four testing conditions without water injection in Channel 2, i.e. both channels are subject to single-phase flow. It can be seen that Channel 1 and Channel 2 have similar flow rates with a difference less than 3%, indicative of identical dimension for the two channels.

#### 3.2. Two-phase flow patterns

Under all the experimental conditions, only film flow patterns were observed in the two-phase flow channel, i.e. Channel 2, as shown in Fig. 6. The presence of liquid film in Channel 2 hampers the air flow by narrowing the air passage, leading to pressure increase. Because only the film patterns were observed, the pressure drop increase is anticipated to correlate with the liquid film thickness. From Fig. 6(a), it is seen that liquid film is developed along the upper side of the channel and dragged towards the outlet by the air flow. As the superficial air velocity increases, the film thickness decreases, as also shown in Lewis and Wang [46] and theoretical estimate [47]. In Fig. 6(b) and (c), liquid film in

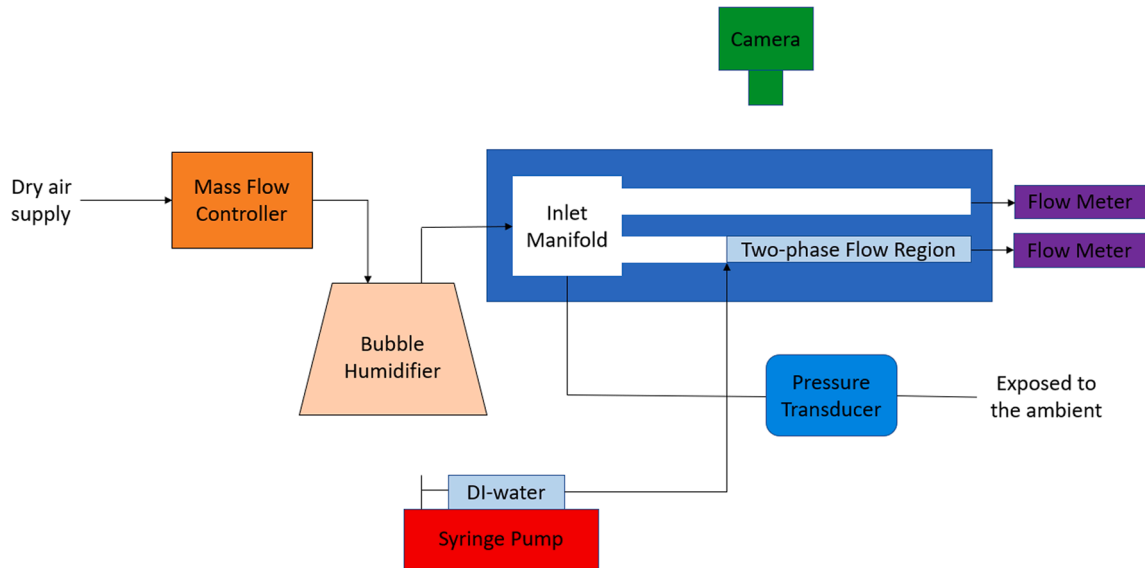


Fig. 3. Schematics of the experimental test section. Channel 1 (the upper channel) is subject to single phase flow, while Channel 2 (the lower channel) is in the two-phase flow regime for the part downstream after the liquid injection port located at the first 1/3 of the channel length.

**Table 1**  
Experimental conditions, physical properties of fluids and channel parameters.

Name	Value	Unit
Air flow rate	100, 150, 200, 250, 300, 350, 400	mL/min
Superficial air velocity	0.86, 1.29, 1.72, 2.15, 2.58, 3.01, 3.44	m/s
Water flow rate	34.99, 3.499, 0.3499	mL/hour
Superficial water velocity	$10^{-2}, 10^{-3}, 10^{-4}$	m/s
Channel dimension	$178(l) \times 3(a) \times 0.324(b)$	mm
Inlet manifold dimension	$12.7 \times 21.6 \times 1.6$	mm
Aspect ratio	$9.259 (a)$	–
Hydraulic diameter	0.585 ( $D_h$ )	mm
Channel cross-section area	0.972 ( $A$ )	mm <sup>2</sup>
Permeability	$9.81 \times 10^{-3} (K)$	mm <sup>2</sup>
Water port location (from the channel inlet)	60	mm
Temperature	20	°C
Outlet pressure	1	Atm

Channel 2 is very thin, i.e. liquid water is drained efficiently out of Channel 2 by air flow. It is also important to note that water tends to accumulate near the outlet of Channel 2, as also observed by Xavier and Wang [32], Lewis et al. [48], Wang et al. [49], and Lu et al. [50]. Lewis and Wang [48] investigated the two-phase flow at the channel expansion to a manifold, indicating that it can significantly increase the overall pressure drop. Wang et al. [49] indicated that channel heterogeneity may cause water accumulation. Lu et al. [50] showed water buildup at the transition area from the channel to exit header of parallel channels.

### 3.3. Gas flow rate ratio $\frac{Q_2}{Q_1}$ and flow maldistribution

The volumetric gas flow rate of each channel was measured when the pressure drop is stabilized. Since Channel 1 only experiences a single-phase flow and the pressure drops in the two channels are always the same, the volumetric flow rate  $Q_1$  in Channel 1 can also be theoretically determined from the pressure measurement through Eq. (5):

$$Q_1 = u_{g1} A \quad (7)$$

where  $u_{g1}$  is the superficial air velocity in Channel 1 and calculated using

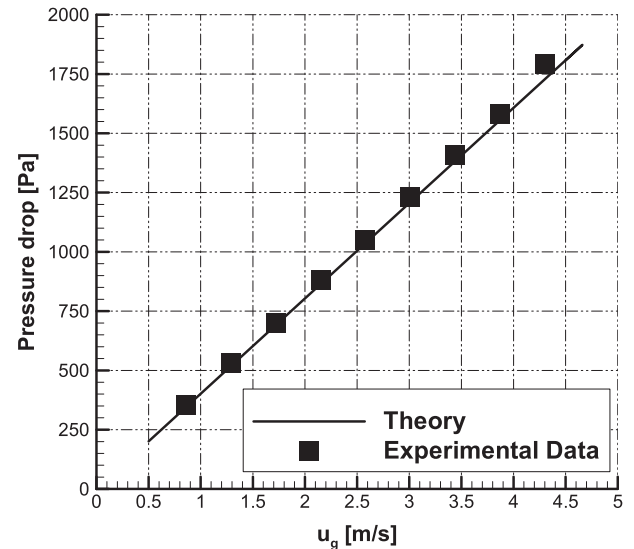


Fig. 4. Gas flow pressure drop for single-phase flow in both channels: theoretical versus experimental data.

Eq. (5) and the experimentally measured pressure  $\Delta P$ . Once  $Q_1$  is determined by the pressure measurement, the volumetric flow rate  $Q_2$  in Channel 2 is then given by:

$$Q_2 = Q_{total} - Q_1 \quad (8)$$

where  $Q_{total}$  is the total flow rate injected into the inlet manifold, which is set at the flow controller. Note that  $Q_2$  in Eq. (8) is obtained from the pressure drop measurement, instead of the direct measurement of the gas flow rate in Channel 2.

To measure flow maldistribution, we define a parameter  $\frac{Q_2}{Q_1}$  as the ratio of the air flow rates in the two channels. A small ratio means severe flow maldistribution. A value approaching to unity means slight maldistribution. In two extreme cases,  $\frac{Q_2}{Q_1} = 1$  corresponds to no maldistribution and  $\frac{Q_2}{Q_1} = 0$  means complete blockage of Channel 2.

In addition, because of the identical cross-sectional areas in Channel 1 and 2, one can reach:

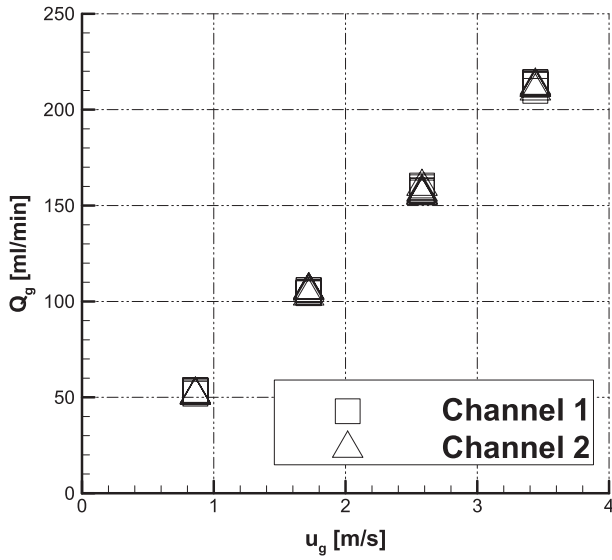


Fig. 5. Measured gas flow rates of the two channels without liquid injection in Channel 2.  $u_g$  is based on the total flow rate and the sum of the two channel cross-sectional areas.

$$\frac{Q_2}{Q_1} = \frac{u_{g2}}{u_{g1}} \quad (9)$$

where  $u_{g_i}$  is the air superficial velocity in Channel  $i$ , which are related to the average superficial gas velocity  $u_g$ ,

$$u_{g1} + u_{g2} = 2u_g \quad (10)$$

In experiment, we also measured  $Q_1$  and  $Q_2$  directly, thus the ratio  $\frac{Q_2}{Q_1}$  can be calculated by these two measurements. Figs. 7a–7c shows the ratio from the direct flow rate measurement of  $Q_1$  and  $Q_2$  as a function of  $u_g$  for the three liquid velocities in Channel 2, respectively. In Fig. 7a, it is seen that the flow rate ratio increases with the air velocity at the superficial water velocity  $u_L = 10^{-2}$  m/s, with a value as high as about 0.65 under the gas velocity of 3.44 m/s. This is because a large air velocity improves liquid removal thereby reducing the liquid film

thickness and its impact on air flow. When the air velocity decreases to 0.86 m/s, the ratio drops to around 0.2, showing that the majority of the air flow takes the pathway of Channel 1 and hence severe maldistribution occurs. As shown in Fig. 6(a) (top), more than half of Channel 2 is filled by liquid water under this air velocity.

Similar trend is observed at  $u_L = 10^{-3}$  m/s for  $u_g > 1.5$  m/s as shown in Fig. 7b. The flow rate ratio reaches 0.7 at the gas velocity of 3.44 m/s. Around  $u_g = 1.5$  m/s, there is a transition, where the trend of the  $\frac{Q_2}{Q_1}$  ratio may take two different directions as  $u_g$  drops to 0.86 m/s with one following the trend of  $u_L = 10^{-2}$  m/s and the other reverse. At  $u_g = 0.86$  m/s, the  $\frac{Q_2}{Q_1}$  value may be around 0.52 or 0.69, depending on the direction of the trend.

Fig. 7c shows the case at  $u_L = 10^{-4}$  m/s, indicating a similar trend for  $u_g > 1.5$  m/s and almost the same ratio (about 0.7) at the highest  $u_g$  as  $u_L = 10^{-3}$  m/s. This is possibly due to the fact that the two-phase

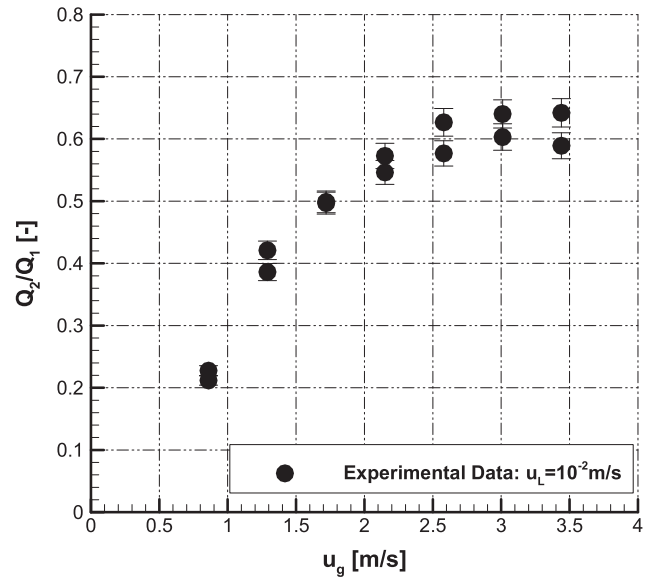


Fig. 7a.  $\frac{Q_2}{Q_1}$  flow rate ratio vs the superficial gas velocity at  $u_L = 10^{-2}$  m/s.

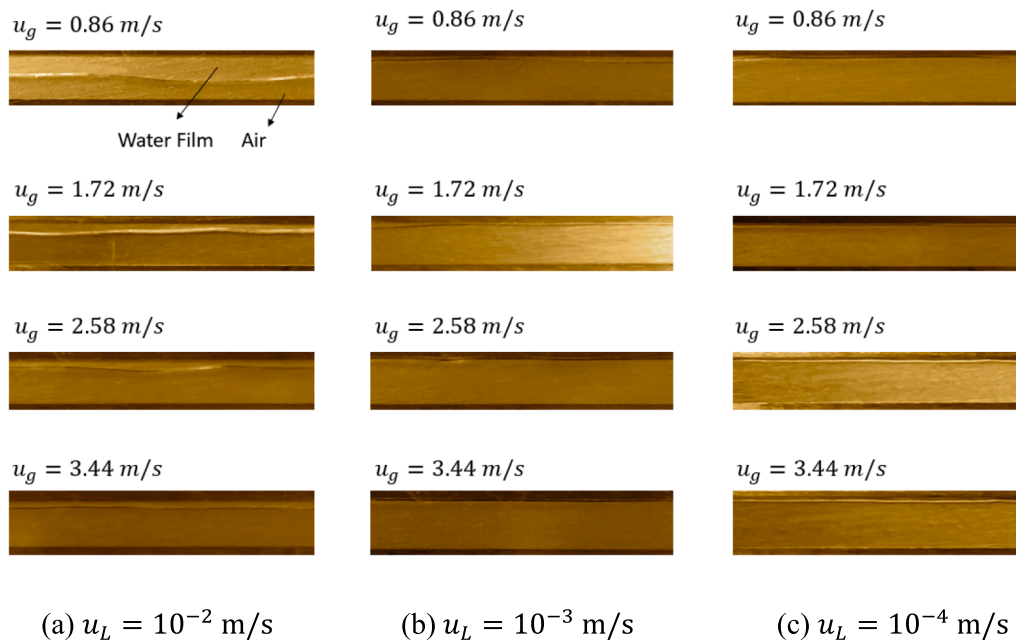


Fig. 6. Visualization of typical two-phase flow patterns in Channel 2.

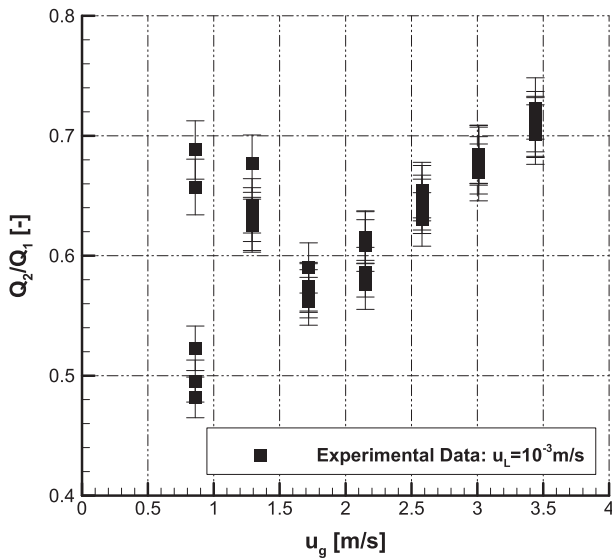


Fig. 7b.  $\frac{Q_2}{Q_1}$  flow rate ratio vs the superficial gas velocity at  $u_L = 10^{-3}$  m/s.

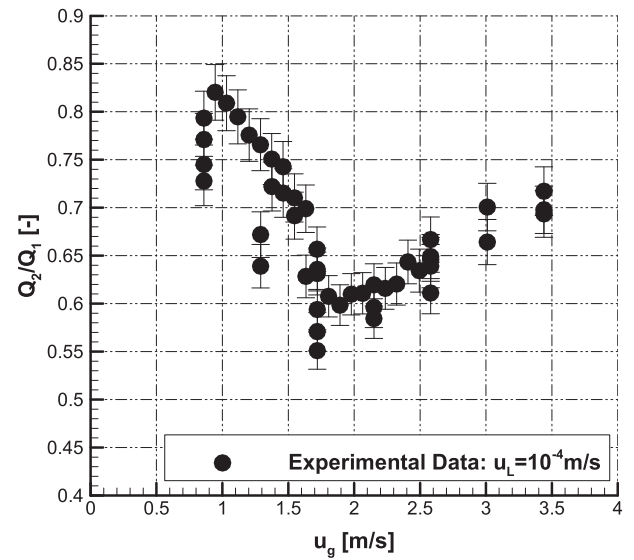


Fig. 7d. Repeating experiment for  $u_L = 10^{-4}$  m/s.

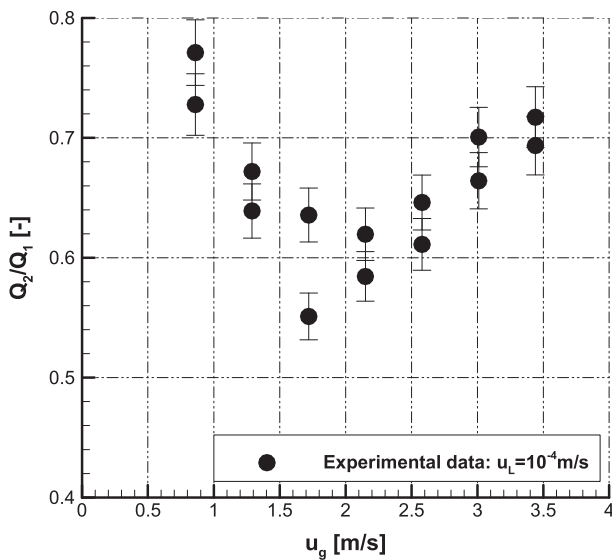


Fig. 7c.  $\frac{Q_2}{Q_1}$  flow rate ratio vs superficial gas velocity at  $u_L = 10^{-4}$  m/s.

dynamics at the outlet plays an important role in the gas flow rate distribution. At the air velocity less than 1.5 m/s, the  $\frac{Q_2}{Q_1}$  ratio only follows the upper path of  $u_L = 10^{-3}$  m/s with the  $\frac{Q_2}{Q_1}$  ratio as high as 0.76 under  $u_g$  of 0.86 m/s. A number of independent repeating experiments were conducted under this  $u_L$ , as shown in Fig. 7d, which confirmed the single path for the air velocity below 1.5 m/s. In addition, the  $\frac{Q_2}{Q_1}$  ratio shows fluctuation at each testing velocity, which is likely due to two-phase flow dynamics. The level of fluctuation is consistent with that observed in other works [46,48].

### 3.4. Exit behavior of two-phase flow and liquid blockage

When the liquid velocity is fixed, the volume fraction of liquid water in the channel region decreases as increase of the gas velocity, as shown in Fig. 6. Thus, it is anticipated that the gas flow ratio  $\frac{Q_2}{Q_1}$  increases with the gas velocity due to the reduced impact by the liquid water. However, this trend is only observed experimentally for the highest water velocity,  $u_L = 10^{-2}$  m/s, as shown in Fig. 7a, while the two other velocities show

different trends. To explore the reason for the different observations, Fig. 8 displays the flow visualization at Channel 2 outlet under  $u_L = 10^{-2}$  m/s with three gas velocities  $u_g = 0.86$  m/s, 1.72 m/s, and 3.44 m/s. It is seen that more liquid water is built up at the outlet under 0.86 and 1.72 m/s, which considerably blocks the gas pathway and causes more maldistribution. At 3.44 m/s, the blockage is less than the other two, as indicated by a wider pathway for gas flow. For  $u_L = 10^{-3}$  m/s and  $10^{-4}$  m/s, the transition region of the  $\frac{Q_2}{Q_1}$  ratio occurs around  $u_g = 1.72$  m/s. Figs. 9 and 10 present the two-phase flow visualizations near the outlet under these two liquid velocities. It is seen that the gas passageway narrows down as the gas velocity increases from 0.86 to 1.72 m/s, as shown in Figs. 9(a) (top) to (b) or 10(a) to (b), then widens as it increases from 1.72 to 3.44 m/s, as shown in Figs. 9(b) to (c) or 10(b) to (c). At  $u_L = 10^{-3}$  m/s and  $u_g = 0.86$  m/s, the outlet may exist at another state of liquid blockage as shown in Fig. 9(a) (bottom), which shows a smaller gas passage than that in Fig. 9(a) (top). Under this condition, the overall pressure drop increases due to the smaller passage, which was also discussed in Ref. [48] for single-channel testing. These two states are attributed to the two “steady” states observed in the ratio  $\frac{Q_2}{Q_1}$ , as shown in Fig. 7b.

It is unclear why the liquid blockage at the outlet is changed or exists at two possible states near  $u_g = 0.86$  m/s for  $u_L = 10^{-3}$  m/s. This may be controlled by the force balance over the liquid at the outlet from the gas drag, gas pressure variation and surface tension, and even the dynamics of gas flows in Channel 1 and 2, and liquid drainage. It is however clearly shown that the flow maldistribution phenomenon is complex in multiple-channel systems.

In addition, the  $\frac{Q_2}{Q_1}$  ratio can also be calculated by directly calculated  $Q_2$  and  $Q_1$  using Eqs. (7) and (8) from direct pressure measurement. Fig. 11 compares the flow rate ratio from the two methods, showing that the data agrees very well under all the testing conditions. To quantify the agreement, we use the mean absolute percent error  $e\%$  defined as:

$$e\% = \frac{1}{n} \sum_{i=1}^n |\Delta r\%| \quad (11)$$

where  $\Delta r\%$  is the difference divided by the average of the two methods.  $e\%$  is calculated less than 4% for the two data sets.

### 3.5. Pressure drop and flow maldistribution

Fig. 12 shows the pressure drop history across the two channels for

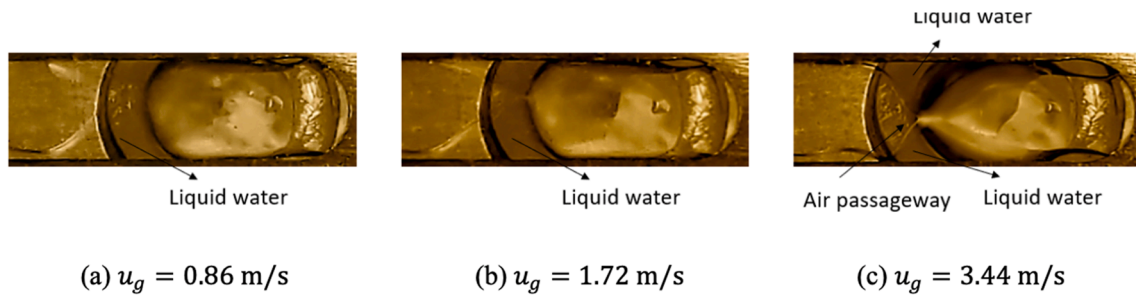


Fig. 8. Typical exit behavior of two-phase flow at  $u_L = 10^{-2}$  m/s.

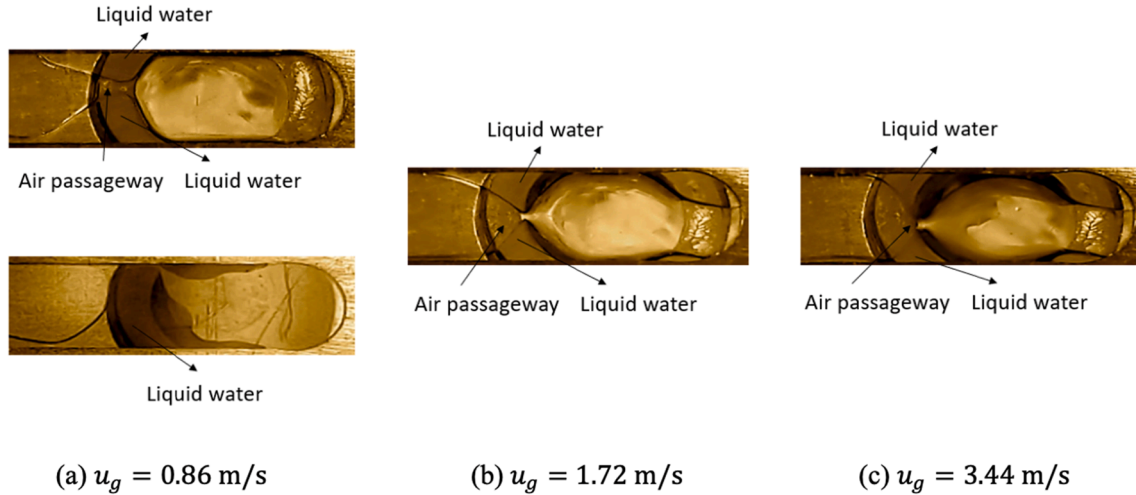


Fig. 9. Typical exit behavior of two-phase flow at  $u_L = 10^{-3}$  m/s.

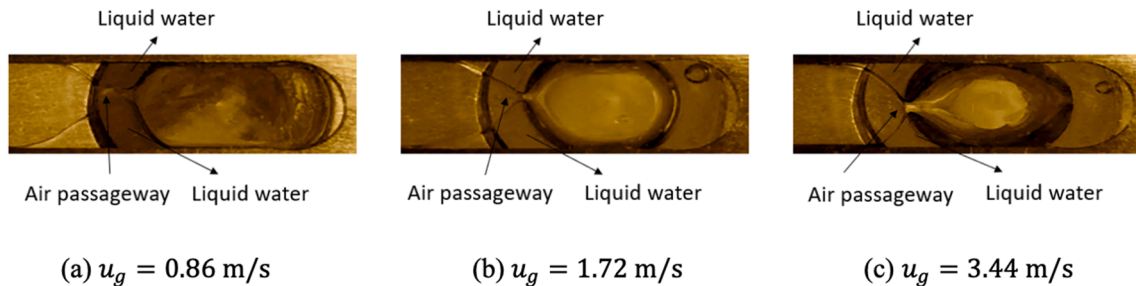


Fig. 10. Typical exit behavior of two-phase flow at  $u_L = 10^{-4}$  m/s.

the entire period of the increasing  $u_g$  test under two superficial liquid velocities:  $u_L = 10^{-3}$  m/s and  $u_L = 10^{-4}$  m/s, respectively. Initially, the single phase flow ran at  $u_g = 0.86$  m/s in both channels till steady state. Then, liquid water was injected to Channel 2 at a constant flow rate with a series of step changes in  $u_g$ . It can be seen that the pressure jumps as the air flow rate steps up. The seven steps, as shown in Fig. 12, correspond to the pressure history at seven different air flow rates, as shown in Table 1. The pressure oscillates greatly at the initial period after  $u_g$  changes, then becomes more stabilized, i.e. the time average is around a constant value. Note that small oscillation still exists at the “stabilized” state, which is probably due to two-phase flow dynamics. Note that the air flow rates,  $Q_2$  and  $Q_1$ , were measured at the “stabilized” states.

Fig. 13a shows the pressure drop measurement against the superficial air velocity from direct  $Q_1$  measurement in Channel 1 in comparison with the theoretical prediction by Eq. (5). It can be seen a good match is achieved. Note that the pressure drop in experiment shows dynamic behavior due to two-phase flow dynamics in Channel 2. The averaged

pressure measurement data in the “steady” state is used to compare with Eq. (5). This figure is also different from Fig. 4, which plots the pressure drop against the single-phase flow velocity averaged over the two channels. The pressure in Fig. 4 is stable because of no influence from two-phase flow. Fig. 13b displays the pressure drop measurement in Channel 2 against the superficial air velocity from direct  $Q_2$  measurement in comparison with other experimental data obtained from a single micro-channel testing [25,26] and the single-phase pressure drop calculated by Eq. (5). As expected, the experimental data lie above the single-phase pressure due to presence of liquid water, which narrows the gas flow passage. In general, the larger the liquid water injection rate, the more the deviation from the single-phase flow pressure. This deviation is the primary cause for flow maldistribution because pressure drives the channel gas flow. Additionally, Fig. 13b presents one set of experimental data per condition to clearly show the trend. Note that the pressure drop may be different under the same condition due to the two-phase flow instability in both channel and outlet, as shown in

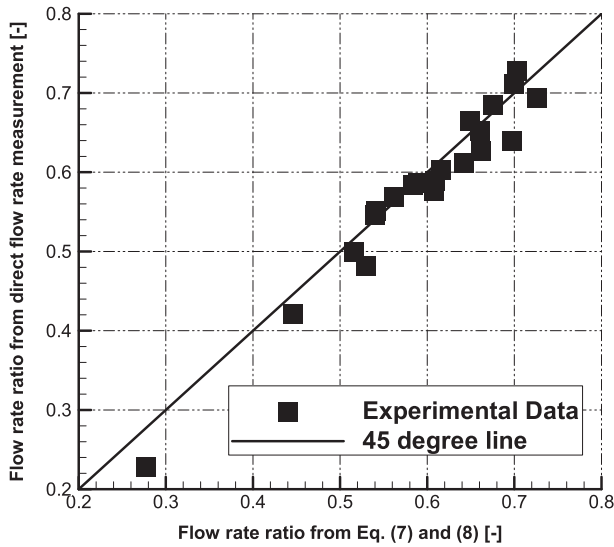


Fig. 11. Gas flow rate ratio  $\frac{Q_2}{Q_1}$  obtained from the direct  $Q_1$  and  $Q_2$  measurement versus that from Eqs. (7) and (8) using the pressure measurement.

Figs. 7a–7d. In addition, the two-phase multiplier ( $\phi$ ) is frequently used to characterize the pressure increase due to presence of the liquid phase, defined by:

$$\phi = \Delta P_{2phase} / \Delta P_{1phase} \quad (12)$$

To obtain this  $\phi$ , a single channel testing usually designed with two separate pressure measurements is carried out: one is under the single phase flow and the other under a two-phase flow.

In this study,  $\phi$  in Channel 2 is not directly calculated. The ratio  $\frac{Q_2}{Q_1}$ , as a direct measure of flow maldistribution, was directly obtained using the direct measurements of either two gas flow rates or the pressure drop and one gas flow rate. This ratio is also directly related to the two-phase multiplier,  $\phi$ , as shown in the below derivation:

From Eq. (5), one can obtain:

$$\frac{\Delta P_{g,Ch1}}{\Delta P_{g,Ch2,1phase}} = \frac{u_{g1}}{u_{g2}} \quad (13)$$

Because Channel 2 is in the two-phase regime, the operational pressure drop is the two-phase pressure,  $\Delta P_{g,Ch2,2phase}$ , given by the  $\phi$  definition:

$$\Delta P_{g,Ch2,2phase} = \Delta P_{g,Ch2,1phase} \phi \quad (14)$$

Because the operational pressure drops in Channel 1 and 2 are always equal at steady state, one will reach:

$$\phi = \frac{Q_1}{Q_2} \quad (15)$$

From the above, the two-phase multiplier  $\phi$  is directly related to  $\frac{Q_2}{Q_1}$ , and thus can be used to directly assess flow maldistribution. A large value of  $\phi$  means a small  $\frac{Q_2}{Q_1}$ , i.e. severe flow maldistribution. The above formula also shows that using the two-channel system in this experiment one can calculate the two-phase multiplier  $\phi$  through direct measurement of the gas flow rates in both channels.

In addition, the two-phase multipliers reported in Lewis and Wang [46,48] are used to calculate the pressure drop in Channel 2, which is also plotted in Fig. 13b for comparison. Note that two multipliers were reported in Lewis and Wang [46,48], including one in the flow channel ( $\phi_1$ ) and the other for both flow channel and outlet expansion ( $\phi_2$ ). To fit with this experiment which has a  $\frac{2}{3}$  length of channel subject to two-

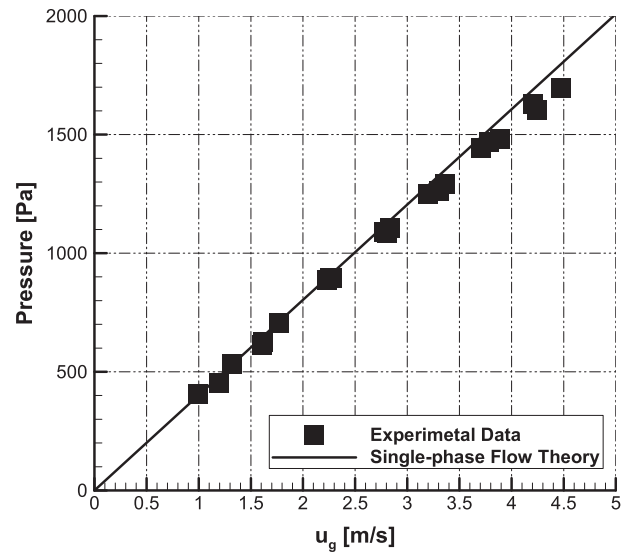


Fig. 13a. Gas pressure drop vs the air velocity in Channel 1.

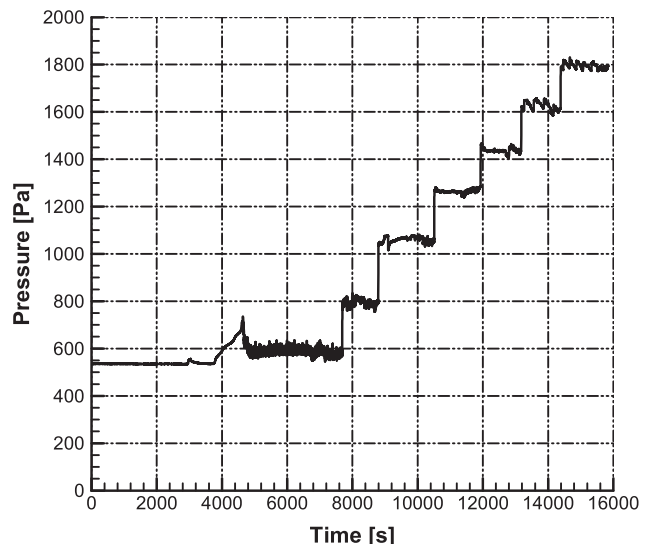
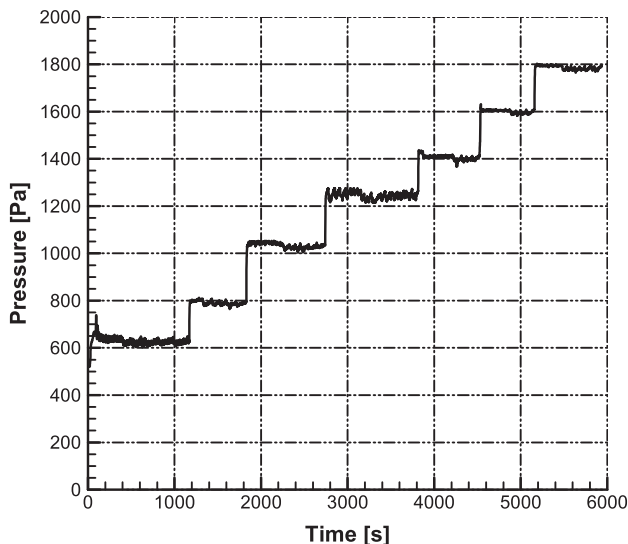


Fig. 12. Typical pressure history in the experiment of: (left)  $u_L = 10^{-3}$  m/s and (right)  $10^{-4}$  m/s, as a function of the gas velocity.

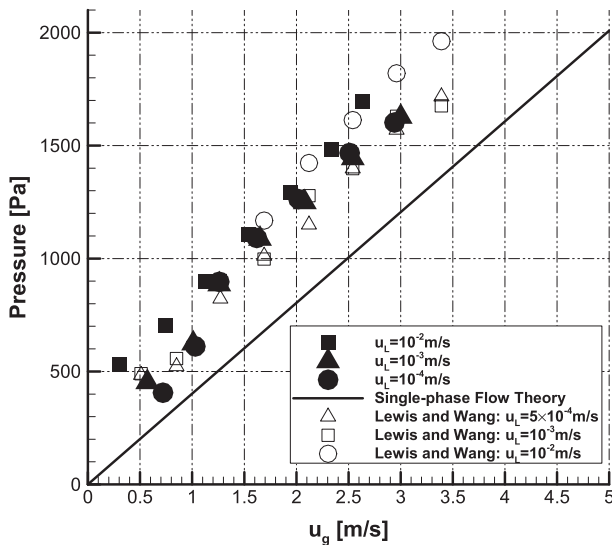


Fig. 13b. Pressure drop vs air velocity in Channel 2 in comparison with experimental results of Lewis and Wang [46,48] and theoretical single-phase pressure drop.

phase flow, the former multiplier ( $\phi_1$ ) in Lewis and Wang [46] was applied to the  $\frac{2}{3}$  portion of Channel 2 in this study. The outlet expansion's effect was accounted by the latter multiplier ( $\phi_2$ ) [48] subtracting the former one ( $\phi_1$ ) [46]. Again, it is seen that the experimental data of the two-phase flow in Channel 2 are in line with the experimental study from literature. However, the single channel testing [46] showed a monotonic change of two-phase multiplier with the gas flow rate for  $u_L = 10^{-4} - 10^{-3}$  m/s, while this present work shows a different changing trend of  $\frac{Q_2}{Q_1}$ . This is possibly due to the fact that in the single channel testing there is no other gas flow path when the channel is almost blocked, while in the multiple-channel case like the present experiment one Channel 1 provides additional pathway for gas flow when Channel 2 is almost blocked. In the single channel testing, when the channel is almost blocked by liquid, the gas pressure will keep increase till pushing the blocking liquid, while in this two-channel testing when Channel 2 is almost blocked its gas flow can bypass blocking liquid via Channel 1. In the latter, the liquid dynamics in the channel and near the outlet will couple with the gas bypass flow dynamics to determine the final flow maldistribution, leading to complex phenomena as observed for  $\frac{Q_2}{Q_1}$ .

4. Conclusion

In this study, a basic system of two parallel thin micro-channels was experimentally investigated to study the fundamentals of liquid water blockage and flow maldistribution. Three liquid water velocities were investigated and discussed to show three representative trends of flow maldistribution. Pressure drop and gas flow rates in individual channels were experimentally measured, along with visualization of the two-phase flow in the channels and outlet.  $\frac{Q_2}{Q_1}$  was defined as a direct measure of flow maldistribution. Specific conclusions are listed below:

- (1) The film flow patterns were observed in Channel 2 for all the operating conditions. It was also shown that the liquid film is thin, almost invisible, under the two low liquid flow rates. In addition, two-phase flow in Channel 2 showed liquid accumulation at the outlet which partially blocks the gas pathway. The outlet two-phase flow may be unstable.
- (2) Gas volumetric flow rates,  $Q_1$  and  $Q_2$ , were measured in individual to calculate  $\frac{Q_2}{Q_1}$ . For  $u_L = 10^{-2}$  m/s, the  $\frac{Q_2}{Q_1}$  ratio was as low

- as 0.2 at  $u_g = 0.86$  m/s and approached to 0.65 at  $u_g = 3.44$  m/s with monotonical increase with the air flow rate. As to  $u_L = 10^{-4}$  m/s, similar trend was observed for  $u_g > 1.72$  m/s. From  $u_g = 1.72 - 0.86$  m/s, the ratio increase from  $\sim 0.6$  to as high as 0.76. As to  $u_L = 10^{-3}$  m/s, similar trend was observed as  $u_L = 10^{-4}$  m/s except two "steady" states were identified at  $u_g = 0.86$  m/s, with one as low as 0.52 and the other as high as 0.69.
- (3) Liquid water tends to accumulate at the Channel 2 outlet and blocks gas flow, which plays an important role in flow maldistribution. Three impacts were observed: at  $u_L = 10^{-2}$  m/s, the blockage monotonically changed with the gas flow rate; at  $u_L = 10^{-4}$  m/s it was observed that  $\frac{Q_2}{Q_1}$  increases when the gas velocity changes from 1.72 to 0.86 m/s. Two states of the blockage at the outlet were observed under  $u_L = 10^{-3}$  m/s and  $u_g = 0.86$  m/s, which were corresponding to the two trends of the  $\frac{Q_2}{Q_1}$  change when the gas velocity decreases from 1.72 to 0.86 m/s.
- (4) The pressure drop evolution showed oscillation at the "steady" state due to the two-phase flow in Channel 2. The direct relationship between the  $\frac{Q_2}{Q_1}$  (or  $\frac{u_{g2}}{u_{g1}}$ ) in the experimental setup and two-phase multiplier  $\phi$  was established, i.e.  $\frac{Q_2}{Q_1} = \frac{1}{\phi}$ . The averaged pressure measurement agreed with the results using the two-phase multiplier reported in literature and the theoretical equation using the gas flow rate measurement  $Q_1$ , respectively. However, it was shown that the two-phase multiplier  $\phi$  obtained in single-channel testing may not be used to calculate flow maldistribution for multiple channels in some cases.

Declaration of Competing Interest

The authors declare that they have no known competing financial interests or personal relationships that could have appeared to influence the work reported in this paper.

Acknowledgement

Y. Wang and J. Wu thank Shanghai Everpower Technologies Ltd for partial financial support.

References

- [1] Y. Wang, K.S. Chen, J. Mishler, S.C. Cho, X.C. Adroher, A review of polymer electrolyte membrane fuel cells: technology, applications and needs on fundamental research, *Appl. Energy* 88 (2011) 981–1007.
- [2] H.W. Wu, A review of recent development: Transport and performance modeling of PEM fuel cells, *Appl. Energy* 165 (2016) 81–106.
- [3] J. Benner, M. Mortazavi, A.D. Santamaria, Numerical simulation of droplet emergence and growth from gas diffusion layers (GDLs) in proton exchange membrane (PEM) fuel cell flow channels, in: ASME 2018 International Mechanical Engineering Congress and Exposition, American Society of Mechanical Engineers Digital Collection, 2018.
- [4] E. Afshari, M. Mosharaf-Dehkordi, H. Rajabian, An investigation of the PEM fuel cells performance with partially restricted cathode flow channels and metal foam as a flow distributor, *Energy* 118 (2017) 705–715.
- [5] Y. Wang, D.F. Ruiz Diaz, K.S. Chen, Z. Wang, X.C. Adroher, Materials, technological status, and fundamentals of PEM fuel cells—A review, *Mater. Today* 32 (2020) 178–203.
- [6] J.T. Thome, Boiling in microchannels: a review of experiment and theory, *Int. J. Heat Fluid Flow* 25 (2004) 128–139.
- [7] M. Aravinthan, S. Sarkar, P. Dhar, S.K. Das, A.R. Balakrishnan, Flow boiling heat transfer characteristics in mini-tubes with and without hydrophobicity coating, *Heat Transfer Eng.* 41 (2020) 288–301.
- [8] K. Zhou, C. Coyle, J. Li, J. Buongiorno, W. Li, Flow boiling in vertical narrow microchannels of different surface wettability characteristics, *Int. J. Heat Mass Transf.* 109 (2017) 103–114.
- [9] N. Guan, Z. Liu, G. Jiang, C. Zhang, N. Ding, Experimental and theoretical investigations on the flow resistance reduction and slip flow in super-hydrophobic micro tubes, *Exp. Therm Fluid Sci.* 69 (2015) 45–57.
- [10] A. Asadollahi, S. Rashidi, J.A. Esfahani, Condensation process and phase-change in the presence of obstacles inside a minichannel, *Meccanica* 52 (2017) 2265–2274.
- [11] Y. Wang, K.S. Chen, S.C. Cho, PEM Fuel Cells: Thermal and Water Management Fundamentals (Sustainable Energy), Momentum Press, 2013.

- [12] N. Ge, S. Chevalier, J. Lee, R. Yip, R. Banerjee, M.G. George, H. Liu, C. Lee, M. Fazeli, P. Antonacci, T. Kotaka, Y. Tabuchi, A. Bazylak, Non-isothermal two-phase transport in a polymer electrolyte membrane fuel cell with crack-free microporous layers, *Int. J. Heat Mass Transf.* 107 (2017) 418–431.
- [13] X. Liu, F. Peng, G. Lou, Z. Wen, Liquid water transport characteristics of porous diffusion media in polymer electrolyte membrane fuel cells: A review, *J. Power Sources* 299 (2015) 85–96.
- [14] H. Markötter, I. Manke, R. Kuhn, T. Arlt, N. Kardjilov, M.P. Hentschel, A. Kupsch, A. Lange, C. Hartnig, J. Scholta, J. Banhart, Neutron tomographic investigations of water distributions in polymer electrolyte membrane fuel cell stacks, *J. Power Sources* 219 (2012) 120–125.
- [15] A. Jayakumar, A comprehensive assessment on the durability of gas diffusion electrode materials in PEM fuel cell stack, *Front. Energy* 13 (2019) 1–14.
- [16] S. Basu, C.Y. Wang, K.S. Chen, Two-phase flow maldistribution and mitigation in polymer electrolyte fuel cells, *J. Electrochem. Energy Convers. Storage* 6 (2009), 031007(1)-031007(11).
- [17] J. Mishler, Y. Wang, R. Mukundan, J. Spendlow, D.S. Hussey, D.L. Jacobson, R. L. Borup, Probing the water content in polymer electrolyte fuel cells using neutron radiography, *Electrochim. Acta* 75 (2012) 1–10.
- [18] T. Cubaud, U. Ulmanella, C. Ho, Two-phase flow in microchannels with surface modifications, *Jpn. Soc. Fluid Mech.* 38 (2006) 772–786.
- [19] Y.C. Zhao, G.W. Chen, Q. Yuan, Liquid-liquid two-phase flow patterns in a rectangular microchannel, *Am. Instit. Chem. Engineers* 52 (2006) 4052–4060.
- [20] S.C. Cho, Y. Wang, Two-phase flow dynamics in a micro hydrophilic channel: A theoretical and experimental study, *70* (2014) 340–352.
- [21] S.C. Cho, Y. Wang, Two-phase flow dynamics in micro channel with heterogeneous surfaces, *Int. J. Heat Mass Transf.* 71 (2014) 349–360.
- [22] P.C. Lee, F.G. Tseng, C. Pan, Bubble dynamics in microchannels, Part I: single microchannel, *Int. J. Heat Mass Transf.* 47 (2004) 5575–5589.
- [23] M.B. Bowers, I. Mudawar, Two-phase electronic cooling using mini-channel and micro-channel heat sinks: Part 2 – flow rate and pressure drop constraints, *J. Electron. Packag.* 116 (1994) 298–305.
- [24] Y. Peles, Two-phase boiling flow in microchannels-instabilities issues and flow regime mapping, *Proceedings of ICMM2003-1069*, pp. 559–566.
- [25] P. Cheng, H.Y. Wu, Phase-change heat transfer in microsystems, *International Heat Transfer Conference 13*, 2006.
- [26] T.S. Ravigururajan, Impact of channel geometry on two-phase flow heat transfer characteristics of refrigerants in microchannel heat exchangers, *J. Heat Transfer* 120 (1998) 485–491.
- [27] A. Salim, M. Fourar, J. Pironon, J. Sausse, Oil-water two-phase flow in microchannels: Flow patterns and pressure drop measurements, *Can. J. Chem. Eng.* 86 (2008) 978–988.
- [28] T.T. Fu, L.J. Wei, C.Y. Zhu, Flow patterns of liquid-liquid two-phase flow in non-Newtonian fluids in rectangular microchannels, *Chem. Eng. Process. Process Intensif.* 91 (2015) 114–120.
- [29] T.A. Trabold, Minichannels in polymer electrolyte membrane fuel cells, *Heat Transfer Eng.* 26 (2005) 3–12.
- [30] F.Y. Zhang, X.G. Yang, C.Y. Wang, Liquid water removal from a polymer electrolyte fuel cell, *J. Electrochem. Soc.* 153 (2006) A225–A232.
- [31] I.S. Hussaini, C.Y. Wang, Visualization and quantification of cathode channel flooding in PEM fuel cells, *J. Power Sources* 187 (2009) 444–451.
- [32] X.C. Adroher, Y. Wang, Ex-situ and modeling study of two-phase flow in a single channel of polymer electrolyte membrane fuel cells, *J. Power Sources* 196 (2011) 9544–9551.
- [33] S. Maharudrayya, S. Jayanti, A.P. Deshpande, Pressure losses in laminar flow through serpentine channels in fuel cell stacks, *J. Power Sources* 138 (2004) 1–13.
- [34] S. Maharudrayya, S. Jayanti, A.P. Deshpande, Flow distribution and pressure drop in parallel-channel configurations of planar fuel cells, *J. Power Sources* 144 (2005) 94–106.
- [35] S. Maharudrayya, S. Jayanti, A.P. Deshpande, Pressure drop and flow distribution in multiple parallel-channel configurations used in proton-exchange membrane fuel cell stacks, *J. Power Sources* 157 (2006) 358–367.
- [36] L.F. Zhang, W. Du, H.T. Bi, D.P. Wikinson, J. Stuper, H.J. Wang, Gas-liquid two-phase flow distributions in parallel channels for fuel cells, *J. Power Sources* 189 (2009) 1023–1031.
- [37] L.F. Zhang, W. Du, H.T. Bi, D.P. Wikinson, J. Stuper, H.J. Wang, Gas-liquid two-phase flow patterns in parallel channels for fuel cells, *J. Power Sources* 189 (2008) 643–650.
- [38] S.G. Kandlika, Z. Lu, W.E. Domigan, A.D. White, M.W. Benedict, Measurement of flow maldistribution in parallel channels and its application to ex-situ and in-situ experiments in PEMFC water management studies, *Int. J. Heat Mass Transf.* 52 (2009) 1741–1752.
- [39] K.K. Nielsen, K. Engelbrecht, D.V. Christensen, J.B. Jensen, A. Smith, C.R.H. Bahl, Degradation of the performance of microchannel heat exchanger due to flow maldistribution, *Appl. Therm. Eng.* 40 (2012) 236–247.
- [40] C. Anbumeenakshi, M.R. Thansekhar, Experimental investigation of header shape and inlet configuration on flow maldistribution in microchannel, *Exp. Therm Fluid Sci.* 75 (2016) 156–161.
- [41] S. Baek, C. Lee, S. Jeong, Effect of flow maldistribution and axial conduction on compact microchannel heat exchanger, *Cryogenics* 60 (2014) 49–61.
- [42] J. Wen, Y.Z. Li, A.M. Zhou, K. Zhang, J. Wang, PIV experimental investigation of entrance configuration on flow maldistribution in plate-fin heat exchanger, *Cryogenics* 46 (2006) 37–48.
- [43] G. Kumaraguruparan, R.M. Kumaran, T. Sornakumar, T. Sundararajan, A numerical and experimental investigation of flow maldistribution in a micro-channel heat sink, *Int. Commun. Heat Mass Transfer* 38 (2011) 1349–1353.
- [44] D.F. Elger, B.C. Williams, C.T. Crowe, J.A. Roberson, *Engineering Fluid Mechanics*, 10 ed., Wiley, 2012.
- [45] S. Kakac, R. Shah, W. Aung, *Handbook of Single-Phase Convective Heat Transfer*, Wiley, 1987.
- [46] J. Lewis, Y. Wang, Two-phase frictional pressure drop and water film thickness in a thin hydrophilic microchannel, *Int. J. Heat Mass Transf.* 127 (2018) 813–828.
- [47] J.E. Steinbrenner, *Two-phase Flow Phenomena in Fuel Cell Microchannels*, Stanford University, 2011.
- [48] J. Lewis, Y. Wang, Investigating the pressure loss associated with two-phase flow in a rectangular microchannel suddenly expanding into a manifold, *Int. J. Hydrogen Energy* 43 (2018) 17444–17460.
- [49] Y. Wang, S. Basu, C.Y. Wang, Modeling two-phase flow in PEM fuel cell channels, *J. Power Sources* 179 (2008) 603–617.
- [50] Z. Lu, S.G. Kandlikar, C. Rath, M. Grimm, W. Domigan, A.D. White, M. Harbarger, J.P. Owejan, T.A. Trabold, Water management studies in PEM fuel cells, Part II: Ex situ investigation of flow maldistribution, pressure drop and two-phase flow pattern in gas channels, *Int. J. Hydrogen Energy* 34 (2009) 3445–3456.
- [51] Y. Wang, Porous-media flow fields for polymer electrolyte fuel cells II. Analysis of channel two-phase flow, *J. Electrochem. Soc.* 156 (2009) B1134–B1141.